Photo-Induced Bending in a Light-Activated Polymer Laminated Composite

Xiaoming Mu[1], Nancy Sowan[2], Julia A. Tumbic[3,4], Christopher N. Bowman[2,5], Patrick T. Mather[3,4], H. Jerry Qi[1*]

[1]*The George W. Woodruff School of Mechanical Engineering, Georgia Institute of Technology, Atlanta, Georgia 30332, USA*

[2]*Material Science and Engineering Program, University of Colorado, Boulder, CO 80309, USA*

[3]*Department of Biomedical and Chemical Engineering, Syracuse University, Syracuse, NY 13244, USA*

[4]*Syracuse Biomaterials Institute, Syracuse University, Syracuse, NY 13244, USA*

[5]*Department of Chemical and Biological Engineering, University of Colorado, Boulder, CO 80309, USA*

*Corresponding author: qih@me.gatech.edu

Abstract

Light activated polymers (LAPs) have attracted increasing attention since these materials change their shape and/or behavior in response to light exposure, which serves as an instant, remote and precisely controllable stimulus that enables non-contact control of the material shape and behavior through simple variation in light intensity, wavelength and spatially controlled exposure. These features distinguish LAPs from other active polymers triggered by other stimuli such as heat, electrical field or humidity. Previous examples have resulted in demonstrations in applications such as surface patterning, photo-induced shape memory behavior, and photo-origami. However, in many of these applications, an undesirable limitation has been the requirement to apply and maintain an external load during light irradiation. In this paper, a laminated structure is introduced to provide a pre-programmed stress field, which is then used for photo-induced deformation. This laminated structure is fabricated by bonding a stretched elastomer (NOA65) sheet between two LAP layers. Releasing the elastomer causes contraction and introduces a compressive stress in the LAPs, which are relaxed optically to trigger the desired deformation. A theoretical model is developed to quantitatively examine the laminated composite system, allowing exploration of the design space and optimum design of the laminate.

1. Introduction

The search for smart materials that respond to external stimuli (such as heat, humidity, magnetic field and light, *etc*.) has drawn great research efforts for decades. Among different stimuli, light provides unique advantages, such as remote activation, spatially controlled activation regions by using a photo-mask or a light-rastering strategy, and instant activation that is easy to stop, pause or resume. In the past, researchers have developed different molecular mechanisms for photo-actuation. The most well-known mechanism is that in liquid crystal elastomers (LCEs) [1-7], which often contain ordered rod-like structures comprised of *trans*-azobenzene moieties. When azobenzene-doped LCEs are irradiated with light of the appropriate wavelength, the bent *cis* form is generated and the sample changes from the ordered nematic phase to the disordered isotropic phase isothermally. The *trans* and *cis* isomers are switched by irradiation with distinct wavelengths of light, which allows contraction or expansion in LCE films [8, 9]. Other polymer systems have also been explored for light activated phenomena. Lendlein et al. [10] developed a crosslinked polymer with photo-tunable molecular crosslinks that can be dimerized to form a secondary crosslink upon irradiation of light of wavelength longer than 260 nm and be cleaved by light of wavelength shorter than 260 nm. The formation and breakage of the secondary network, when coupled with proper mechanical deformation, facilitated a reversible shape memory effect [11]. Scott et al. [12, 13] also developed an amorphous, covalently crosslinked polymer network, in which light irradiation cleaves the embedded photoinitiators into free radicals that initiate bond exchange reactions (BERs), where a polymer chain with a radical at one end first adds into a bond on a neighboring chain to form a tertiary radical structure, followed by fragmentation of an adjacent bond to transfer the radical to a new free chain. As this alternating bond formation and breaking process continues, the polymer network rearranges until radical-radical termination occurs. Such events permanently alter the polymer network structure and restore the polymer network to its highest entropy

configuration. Mechanically, this network rearrangement is able to relax the prestresses that exist in the material. Previous work has shown potential applications of BERs in polymers, generally termed light-activated polymers (LAPs), including surface patterns, flaw retardation and light-reforming [14-17]. Further, constitutive models have been developed to describe BERs for such covalently adaptable polymer networks [17-20]. Despite this progress, one drawback of such polymer systems is that the material has had to be maintained in a stressed state for light exposure to trigger actuation. The same drawback can also be found in applications of the photoreversible material developed by Lendlein et al. [10]. This necessity is normally achieved by application of an external load during irradiation. It is not hard to imagine that such a requirement imposes some limitations in some applications such as photo-origami [21].

Origami is a traditional handicraft that starts with a flat sheet of paper and finishes with a vivid three-dimensional (3D) structure through folding and shaping [22-24]. Motivated by origami, researchers use smart materials as "paper" and stimulus as "hands" to deform materials into 3D structures for potential engineering applications, such as shopping bag packaging, aerospace structures, photovoltaic, and biomedical devices [23, 25-30]. Shape memory polymers have recently been introduced as a platform for origami [31-34] on the basis of their unique shape memory effect. Photo-origami [21], involving light-induced folding, is immediately attractive for its non-contact, spatially resolved potential; however, the required mechanical force during light irradiation clearly compromises the advantage of remote actuation in photo-origami. One solution to overcome this hurdle is to introduce and store some elastic energy into LAPs by using a laminated structure that is illuminated on one side, asymmetrically releasing the stored elastic energy and curling the laminate. In such a configuration, no external load is necessary and self-folding that is activated solely by light is possible. Although we only studied the photoactivated covalent adaptive network developed by Scott et al. [12, 13] for the present work, the same strategy should be applicable to the photoreversible

4

material of Lendlein. This paper demonstrates the feasibility of using such a concept for light-activated bending, which could then be used as a hinge for future origami design. We further explore the design space for maximizing the bending deformation. The paper is organized as follows. Section 2 introduces materials and experiments, while light propagation, chemical reaction kinetics and our theoretical model are presented in Section 3. Simulation results together with experimental results are compared in Section 4. Based on the theoretical model, a parametric study is also presented in this section to explore the design space and optimize the bending curvature. Section 5 concludes the work.

2. Materials and Experiments

2.1 Materials

The laminate (which will be discussed in Section 2.3) consists of two LAP layers and an intermediate elastomer layer. The monomers used for the LAPs include pentaerythritol tetra(3–mercaptopropionate) (PETMP) and ethylene glycol di(3–mercaptopropionate) (EGDMP), which were donated by Bruno Bock Thiochemicals. The monomer 2-methylene-propane-1,3-di (thioethylvinylether) (MDTVE), was synthesized from 2-chloroethyl vinyl ether and 3–mercapto–2–(mercaptomethyl)–1–propene [35]. The photoiniatiators Irgacure 184 (1–hydroxy–cyclohexyl–phenyl–ketone) and Irgacure 819 (bis(2,4,6–trimethylbenzoyl)–phenylphosphineoxide) as well as the UV light absorber Tinuvin 5060 (2-(2-hydroxyphenyl)-benzotriazole) were obtained from BASF (formally Ciba) and were used without further treatment. LAPs synthesis was achieved in a manner similar to previous work by Bowman and coworkers [12, 13]. A spot UV curing lamp (OmniCure S2000, Lumen Dynamics, Ontario, Canada) equipped with bandpass filters was used for all light exposures. Intensities were measured by a radiometer (IL1400A, International Light Technologies, Peabody, MA). The networks were formulated by adding two kinds of photoinitiators Irgacure 184 (1.0 wt%) and Irgacure 819 (1.0 wt%)

into a mixture of PETMP, MDTVE and EGDMP in a weight ratio 1:5:4. This formulation is "optically thin" [36] such that the light intensity is approximately uniform through the thickness for the film geometry used (see below). This mixture was stirred for 5 min at 45 °C to achieve homogeneity and then immediately sandwiched between two glass slides coated with Rain-X (SOPUS Products, Houston, TX) and separated by 0.13 mm polyester shims. This uncured, formulated resin was irradiated by light of 400-500 nm wavelength at 40 mWcm^{-2}, which photocleaves Irgacure 819 into radicals and initiates the polymerization via a radical-mediated thiol-ene reaction. Irgacure 184, which is incorporated for later photoactivation, does not absorb light of 400-500 nm wavelength and was not consumed during the photopolymerization. Another, "optically thick" network was fabricated with an additional 3 wt% Tinuvin 5060 before polymerization. This second network solution was designed for use as a thin adhesion layer during lamination. Since it also greatly attenuates light intensity, it can block the light and create a relatively unexposed region underneath.

A commercially formulated optical resin, NOA65 (distributed by the Norland Products Incorporated Company, Cranbury, NJ), was selected for the intermediate layer in the laminated composite and was used as purchased. NOA65 is a photopolymer that cures by UV light at 350-380 nm wavelength range to a final T_g below room temperature and, thus exists as an elastomer at ambient conditions. We injected the uncured liquid resin into glass slides with 0.17 mm spacing shims and cured it under 365 nm UV light at 20 mWcm^{-2} for 2 h. Glass slides were flipped over every 30 min to ensure the resin was fully cured.

2.2 Mechanical and Photomechanical Characterization

For photomechanical testing, an optically thin LAP sheet was cut into strips (15 mm (L) ×4 mm (W) ×0.13 mm (T)). Stress relaxation tests were conducted using a dynamic mechanical analyzer (Q800 DMA, TA Instruments, New Castle, DE). Each sample

mounted between film tension clamps with a static preload force of 0.001 N. Samples were stretched to 10% strain in the strain rate mode of the instrument and a strain rate of 5%/min. After being held in that strained state for 2 min, the sample was irradiated by a 365 nm UV light for 15 min and the holding force was measured during this time. Light intensity was varied to include 5 mWcm^{-2}, 10 mWcm^{-2}, 20 mWcm^{-2} and 40 mWcm^{-2}.

2.3 Laminate fabrication

Figure 1 shows the fabrication procedure of the laminated composite. A NOA65 strip was first fixed by the clamps and then stretched and maintained at a fixed strain during the adhesion. Two optically thin LAP strips as described above, shorter in length than the deformed NOA65 strip, were bonded to the stretched intermediate layer by using optically thick LAP solution as adhesive and cured upon exposure to 400-500 nm light at 40 mWcm^{-2}. After releasing the two ends, the laminated composite shrank due to the contraction of the intermediate, elastomeric layer. The gripped two ends were carefully cut off, yielding a laminated composite with each layer of the same length and width and with the central, elastomeric layer existing under tension and the outer LAP layers existing in a state of compression. The laminated composite thus prepared was irradiated by light from one side with an expectation of actuation as light relaxes the compressive stress of the layer facing the light source. Photos of the experimental arrangement used can be found at Figure S1 in the supporting information.
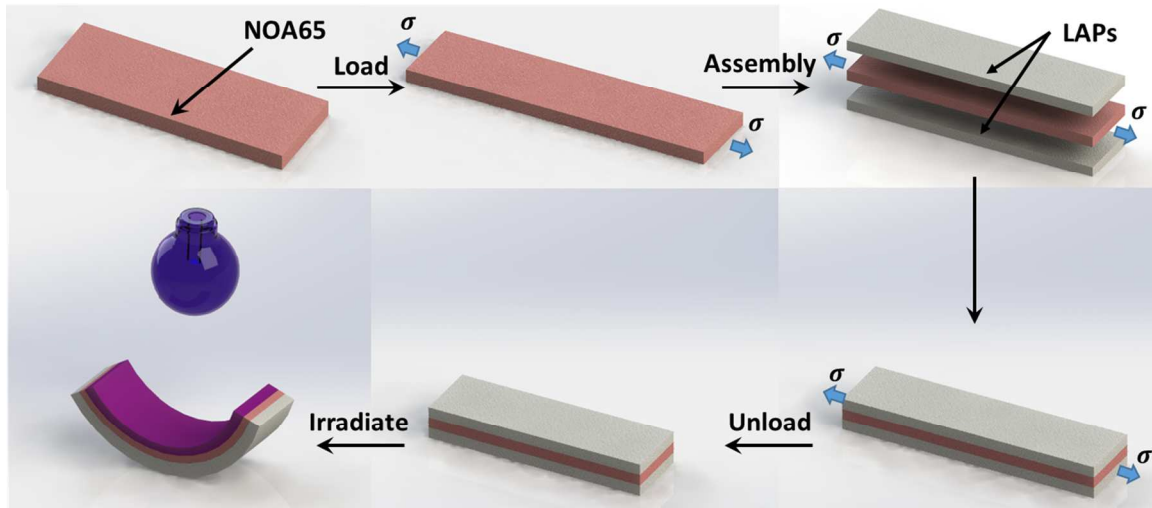
Figure 1. Fabrication and activation process of laminated structure. Step 1: the NOA65 layer was first loaded uniaxially; Step 2: two LAP layers were then bonded on both sides of the stretched NOA65 layer; Step 3: the intermediate layer was released; Step 4: the top LAP layer was irradiated.

3 Modeling the photomechanics and photo-actuation of the laminate

We developed a theoretical model to predict the nature and magnitude of light-induced laminate curvature. As light propagates through the top-most LAP layer, photons react with the embedded photoinitiators, generating free radicals that subsequently initiate BERs that lead to macroscopic relaxation of the compressive stress applied by the elastomeric central layer to which it is bonded. Since the LAPs are on the outer layer of the laminate, this stress-relaxation causes the laminate to bend. Therefore, the bending curvature is controlled by light propagation, radical generation, BER rate, laminate dimensions, mechanical properties of each layer in the laminate, and the initial mechanical loading. To study the complicated interrelationship among these factors, we start with the physics of light propagation and then describe briefly a photomechanical model for LAPs, which is finally substituted into the laminated structure, incorporating the geometric attributes and the mechanical properties, to predict the bending.

3.1 Light propagation

For the physics of light and constitutive behavior of the LAPs, we follow the previous work [36] where the system modeled is composed of LAPs network, photoinitiators, radicals and photoabsorbers and phase evolution theory is used [18] to describe stress relaxation caused by BERs. Since we are interested in the laminated structure described above, the system can be simplified as a two-dimensional (2D) problem, depth and length. Therefore, all the equations will be written in their 2D form. Here, we assume that light penetrates through the material along its thickness direction (z-direction), which is measured with *z*=0 at the light entering surface. Light propagation through a continuous media is described by the Beer-Lambert law,

$$\frac{\mathrm{d}I(z,t)}{dz} = -A(z,t)I(z,t), \tag{1}$$

where $I(z,t)$ is the intensity of light and is a function of spatial coordinate and time; $A(z,t)$ is the extinction field that describes the spatial variation of light due to absorption. The extinction field in the current study is characterized as,

$$A(z,t) = \alpha_I C_I(z,t) + A_{matrix}, \tag{2}$$

where α_I is the absorptivity of photoinitiators; $C_I(z,t)$ is the concentration field of initiators; A_{matrix} is the absorption from other species in the matrix, such as Tinuvin 5060. Since we are only concerned with the optically thin layer, A_{matrix} is set to zero. Based on Fresnel's equations, Snell's law and the Beer-Lambert law, the light intensity field in a curled LAP optically thin sample was computing using MATLAB and the results are shown in the supporting information Figure 2S. To simplify this simulation, we neglect the possibility that the light reflected on the entering surface may continue irradiating other areas of the top surface, and also ignore the effect of the light reflected from the bottom surface, which would lead to repeated internal reflections in the laminate. Moreover, the final curled shape with initial concentrations of photoinitiators is studied (instead of the initial flat configuration with decaying photoinitiator concentration) so

that the bending deformation of the laminate can also be taken into consideration. As the results show in Figure S2, the lowest intensity for this extreme scenario is located at the two ends and is still 82% of the incident light. Thus, we assume hereafter that light intensity is uniform in the LAPs during irradiation and is not affected by the bending deformation of the laminate. For larger bending angles, a nonlinear approach where the incident angle varies and the reflection and deflection of light due to the surface will have to be considered.

3.2 Photochemistry

During UV irradiation, light propagation through LAPs induces photochemical reactions on photoinitiator molecules, generating free radicals, cleaving and reforming polymer backbone through BERs. The photoinitiator consumption and free radical generation are governed by:

$$\frac{\partial C_I(z,t)}{\partial t} = -\beta C_I(z,t)I(z,t) + D_I \nabla^2 C_I(z,t), \qquad (3)$$

$$\frac{\partial C_R(z,t)}{\partial t} = m\beta C_I(t)I(z,t) - k_{term}\big(C_R(z,t)\big)^n, \qquad (4)$$

where $C_I(z,t)$ and $C_R(z,t)$ are the concentrations of photoinitiators and free radicals; β is a lumped constant parameter representing absorption and quantum efficiency; m is the number of free radicals generated from one initiator and is precisely 2 in the current study. The second term on the right hand side (RHS) of Eq. 3 describes the diffusion of photoinitiator with D_I diffusivity. The second term on the RHS of Eq. 4 captures the termination of free radicals where prefactor k_{term} is a fitting parameter and exponent n defines the number of radical molecules for each termination reaction. Although bimolecular termination was expected, the value of n is estimated as unity experimentally [13, 36] . Since free radicals diffuse much more slowly than photoinitiators, the diffusion of free radicals is not considered.

3.3 Photo-induced stress relaxation

Irradiation initiates BERs that rearrange the polymer network. Here, we use the well-developed phase evolution rule [18] to describe the network rearrangement and its mechanical consequences:

$$\frac{\partial f_O(z,t)}{\partial t} = -k_1 C_R(z,t) f_O(z,t)^p, \tag{5}$$

$$f_O(z,t) + f_R(z,t) = 1 \tag{6}$$

where f_O and f_R are the volume fraction of the original network and reformed network, respectively; k_1 is a fitting parameter and the negative sign indicates the decrease of the original network fraction due to reformation; the power p is also a fitting parameter that captures the dependency of the rate on the volume fraction of the original network.

We assume that $t = 0$ is the time before which there is no irradiation and at which point irradiation begins. The stress in the LAPs is,

$$\sigma_0 = E_L \varepsilon_L^0, \tag{7}$$

where ε_L^0 is the initial strain and E_L is the modulus of the LAP. Here, the subscript L indicates reference to the LAP layers. In addition, we use the Hencky strain $\varepsilon = \ln\lambda$ as it conveniently converts the multiplication of stretches into additive strains and thus simplifies the numerical calculations [37].

After $t = 0$, light irradiation starts and triggers BERs. The mechanical stress in the LAPs during light irradiation can be described generally as [20, 38],

$$\sigma(z,t) = E_L\big(1 - f_R(z,t)\big)\big(\varepsilon_L^0 + \Delta\varepsilon(z,0,t)\big) + E_L \int_0^t \frac{\partial f_R(z,\tau)}{\partial \tau} \Delta\varepsilon(z,\tau,t)d\tau, \tag{8}$$

where $\Delta\varepsilon(z, 0, t)$ is the strain increment during light irradiation, or from time 0 (when the irradiation starts) to time t; $\Delta\varepsilon(z, \tau, t)$ is the strain increment measured from time τ to time t.

3.4 Model for the laminated structure

As illustrated in Figure 1, the intermediate layer is loaded to a pre-determined strain and held at that strain while the two LAP layers are attached. After releasing the external load, the laminate shrinks due to the contraction of the intermediate layer and compressive strain is thus introduced in the LAP layers. The thickness of the LAP layer is re-measured after the fabrication of laminated composite to take the thickness of each bonding layer into account. In this section, we develop a model to describe the photo-induced laminate bending.

3.4.1   Laminate contraction

The first step in the model is to predict the compressive strain in the LAP layers induced by unloading the intermediate layer. This can be obtained simply by using the equilibrium equation,

$$E_N(\varepsilon_0 + \varepsilon_N)h_N + 2E_L\varepsilon_L h_L = 0, \tag{9}$$

where E_N is the modulus of the intermediate NOA65 layer; ε_0 is the initial strain in the intermediate layer; h_N and h_L are the thicknesses of intermediate and the LAP layers, respectively; ε_N and ε_L are the strain increments in intermediate and LAP layers, respectively. Assuming there is no slip on the interfaces, the strain increments in each layer should be identical $\varepsilon_N = \varepsilon_L$. Also, note that this strain is the initial mechanical strain (prior to illumination) in the LAP layers, thus

$$\varepsilon_L^0 = \varepsilon_L = -\varepsilon_0/[1 + (2E_L h_L)/(E_N h_N)]. \tag{10}$$

The negative sign here indicates that the LAP layers are under compression. As expected, a larger initial tensile strain in the intermediate layer, ε_o, creates a larger compressive strain in the LAP layers. The final compressive strain in the LAP layers also depends on material properties and geometric parameters. Generally, a thicker and stiffer intermediate layer is able to introduce more compressive strain in the LAP layers.

3.4.2   Laminate bending

The laminate consists of three layers, whose dimensions of the cross-section are shown in Figure 2a, where x-y is in the plane of the LAP layer that is irradiated and the z coordinate defines the thickness. The bending angle is defined as θ in Figure 2b with an initial value 0° when laminate is flat. Based on Euler-Bernoulli beam theory, taking the strain at $z=0$ as ε_0 ($\varepsilon(0) = \varepsilon_0$), strains along z axis due to bending are as follows,

$$\varepsilon_b(z,t) = \varepsilon_0(t) + \kappa(t)z, \tag{11}$$

where κ is the bending curvature of the beam. It should be noted that $z=0$ is not the neutral axis, and therefore ε_0 is not necessarily zero. Since the bending is caused by light irradiation, the bending strain is equal to the strain increment. Thus

$$\Delta\varepsilon(z,0,t) = \varepsilon_b(z,t) = \varepsilon_0(t) + \kappa(t)z, \tag{12}$$

$$\Delta\varepsilon(z,\tau,t) = \varepsilon_b(z,t) - \varepsilon_b(z,\tau) = \varepsilon_0(t) - \varepsilon_0(\tau) + [\kappa(t) - \kappa(\tau)]z. \tag{13}$$

The above two equations can be used directly to calculate the stress in the irradiated LAP layer by using Eq. 8. For the unirradiated LAP layer and the intermediate layer, the strains are

$$\varepsilon_U(z,t) = \varepsilon_L^0 + \Delta\varepsilon(z,0,t) = \varepsilon_L^0 + \varepsilon_0(t) + \kappa(t)z, \tag{14}$$

$$\varepsilon_N(z,t) = \varepsilon_0 + \varepsilon_L^0 + \Delta\varepsilon(z,0,t) = \varepsilon_0 + \varepsilon_L^0 + \varepsilon_0(t) + \kappa(t)z, \tag{15}$$

where the subscript U represents the unirradiated LAP layer and the subscript L in the following equations notes the irradiated LAP layer.

The stresses in the unirradiated LAP layer and the intermediate layer can be calculated as

$$\sigma_U(z,t) = E_L \varepsilon_U(z,t), \tag{16}$$

$$\sigma_N(z,t) = E_N \varepsilon_N(z,t). \tag{17}$$

(a)   (b)
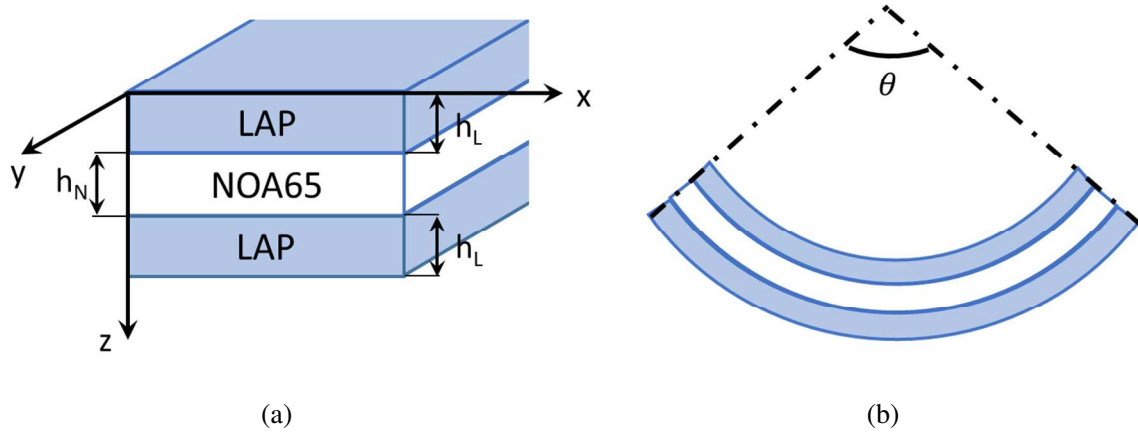
Figure 2. Geometry: (a) Cross-section, and (b) Bending angle θ of the laminate.

In the above equations, $\varepsilon_0(t)$ and $\kappa(t)$ are the two unknowns and are solved by checking force and moment equilibrium along the beam cross-section. During irradiation, there are no external forces or moments acting on the laminate. In order to meet force and moment equilibrium, we have,

$$F_{total} = F_U + F_N + F_I = 0, \tag{18}$$

$$M_{total} = M_U + M_N + M_I = 0, \tag{19}$$

where F_N, F_U and F_I are the forces acting on the cross-section of intermediate layer, unirradiated and irradiated layers, respectively. Substituting Eq. 8, Eq. 16 and Eq. 17 into the above equilibrium equations, we obtain:

$$\int_0^{h_L} \sigma_I(z)dz + \int_{h_L}^{h_L+h_N} \sigma_N(z)dz + \int_{h_L+h_N}^{2h_L+h_N} \sigma_U(z)dz = 0, \tag{20}$$

$$\int_0^{h_L} \sigma_I(z)zdz + \int_{h_L}^{h_L+h_N} \sigma_N(z)zdz + \int_{h_L+h_N}^{2h_L+h_N} \sigma_U(z)zdz = 0, \tag{21}$$

The above two equations are solved incrementally for $\varepsilon_0(t)$ and $\kappa(t)$. Once the curvature has been determined at each time-point, the bending angle can be simply solved for using the expression,

$$\theta(t) = \kappa(t)L \tag{22}$$

where L is the length of the irradiated region. L is set to be 1 mm to calculate the bending angle of a 1 mm long laminated composite ($^\circ$ mm^{-1}) in the next section. This facilitates comparison with experiments for any L.

4   Results

The above theoretical model was implemented into a MATLAB program. Three fitting parameters were first determined based on the stress relaxation tests of the LAPs. Then the theoretical model was used to simulate laminate bending and compare with experimental results. Finally, a parametric study was done to explore the optimum bending curvature.

4.1 Photo-induced stress relaxation for LAP material parameters

Photo-induced stress relaxation tests were conducted by using the DMA apparatus at various light intensities: 5, 10, 20, and 40 mWcm^{-2} as described in Section 2.2. The normalized stress relaxation curve at 10 mWcm^{-2} was used to determine the three fitting parameters; namely, the radical termination rate k_{term}, the phase evolution prefactor k_1 and the power p. The rest of the parameters in the model for the LAP were obtained from

the literature [36]. Having established all of the necessary parameters, the other three curves were predicted for comparison with experiment using the same parameter set, as shown in Figure 3. The fitting parameters are shown in Table 1 with other parameters and their references. These parameters were then used in the laminate bending simulations as will be shown in the following subsection.
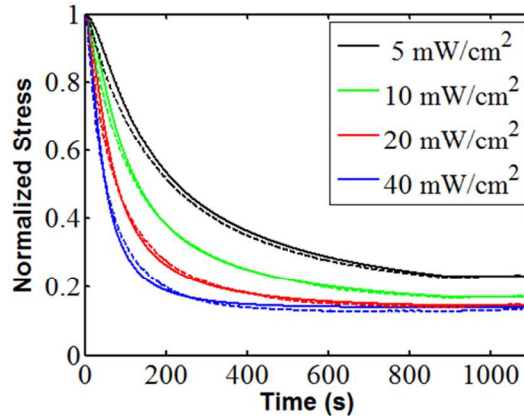
Figure 3. Phase evolution theory is used to predict photo-induced stress relaxation at various light intensity: solid lines are simulation results and dash lines are experimental results.

Figure 3 shows a good agreement between the model simulations and the experimental results. In general, a higher light intensity causes a faster stress relaxation rate and, overall, stress relaxation occurs slowly, on the order of minutes during illumination. Use of a high light intensity such as 40 mWcm^{-2} can speed up the response time and relax the stress within 4 min. However, doing the higher light intensity leads to heating and other secondary processes that may be undesirable and lead to less control of the ratio of stress relaxation at the top and bottom interfaces. Thus, to achieve the greatest control and maximize the relative stress relaxation at the two surfaces, we chose a lower light intensity, i.e., 10 mWcm^{-2}, in the laminate bending experiment. Use of this intensity can relax the same amount of stress as occurs at the high light intensity; however, a greater level of control and ideality is observed in the process.

Table 1. Parameters used in the theoretical model are listed along with reference from which the value

was obtained ("Calculated" means that it is calculated from the information provided by the vendor).

Parameter	Value	Units	Description	Reference
α_I	118	L mol^{-1} cm^{-1}	Photoinitiator molar absorptivity	[36]
$C_I(0)$	0.047	mol L^{-1}	Initial photoinitiator concentration	Calculated
A_{matrix}	0	cm^{-1}	Photoabsorber coefficient	[36]
$C_R(0)$	0	mol L^{-1}	Initial radical concentration	Calculated
m	2	Dimensionless	Number of radicals generated per initiator	[36]
β	1.8e-5	s^{2}kg^{-1}	Photoinitiation coefficient	Calculated
k_{term}	0.03	s^{-1}	Radical termination prefactor	Fitted
n	1	Dimensionless	Radical termination exponent	[36]
k_1	2.0	Dimensionless	Phase evolution prefactor	Fitted
p	2.0	Dimensionless	Phase evolution exponent	Fitted
E_L	4.1	MPa	LAPs modulus	Measured
E_N	6.7	MPa	NOA65 modulus	Measured

4.2 Experimental and theoretical results

A 0.17 mm thick NOA65 strip with an initial length approximately 9.10 mm was stretched to 10.47 mm (15% strain) and held at that deformation during the adhesion step. After assembly, the laminated composite was released, contracting to a length of 9.73 mm and remaining flat, as expected due to the symmetric assembly. The thickness of the laminated composite was then measured as 0.51 mm, revealing a final thickness of the LAP layer (including bonding part) was 0.17 mm. The laminated composite was then irradiated on one side by 365 nm, 10 mWcm^{-2} light. Figure 4 shows the bending of the laminated composite during light irradiation from the top-side. A digital camera was set up to take photos every 15 seconds during irradiation. Selected photos with a time

interval of 2 minutes are presented in Figure 4 and the video can be found as Video S1 in the supporting information. As the figure shows, the initially flat laminate exhibited noticeable bending curvature after 2 min irradiation. Curvatures and bending angle per unit length at different times were measured by ImageJ and are shown in Figure 5a and 5b. The bending curvature of the laminated composite gradually increased to 0.163 mm^{-1} at 10 min and then slowly approached 0.175 mm^{-1} by 15 min when the whole laminate bent 90°. In addition, due to the uniform irradiation on the top surface, the laminate shows an almost uniform bending curvature.
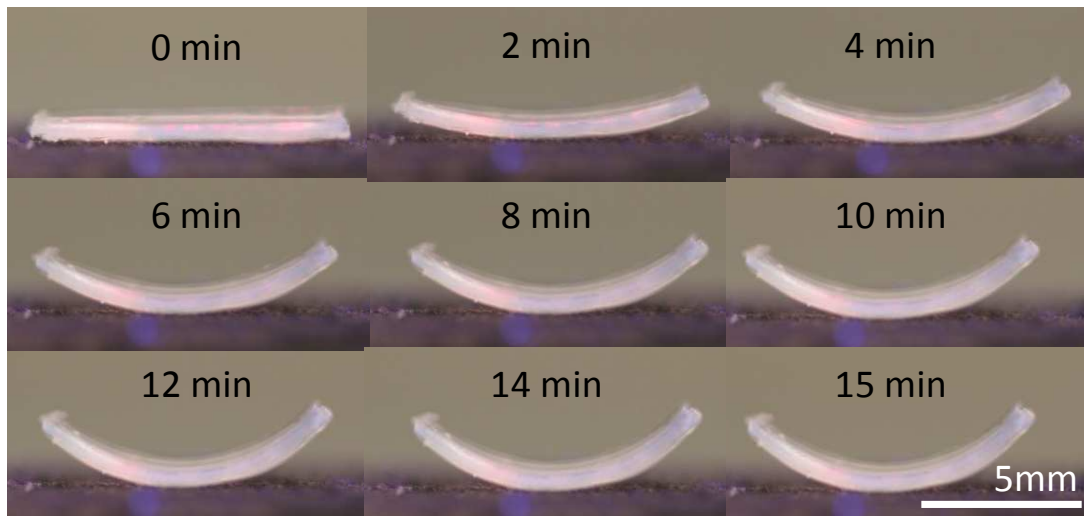
Figure 4. Laminate bending behavior upon 10 mWcm^{-2}, 15 minutes UV irradiation.

It is shown in Figure 5a that the curvature increases nonlinearly with the irradiation time and approaches a plateau at the end of the irradiation, attributed to the nonlinear stress relaxation of the LAPs as shown in Figure 3. The bending angle in the current laminate asymptotes at 10° mm^{-1}, as shown in Figure 5b. We observed further that the theoretical predictions match well the experimental results.

(a)   (b)
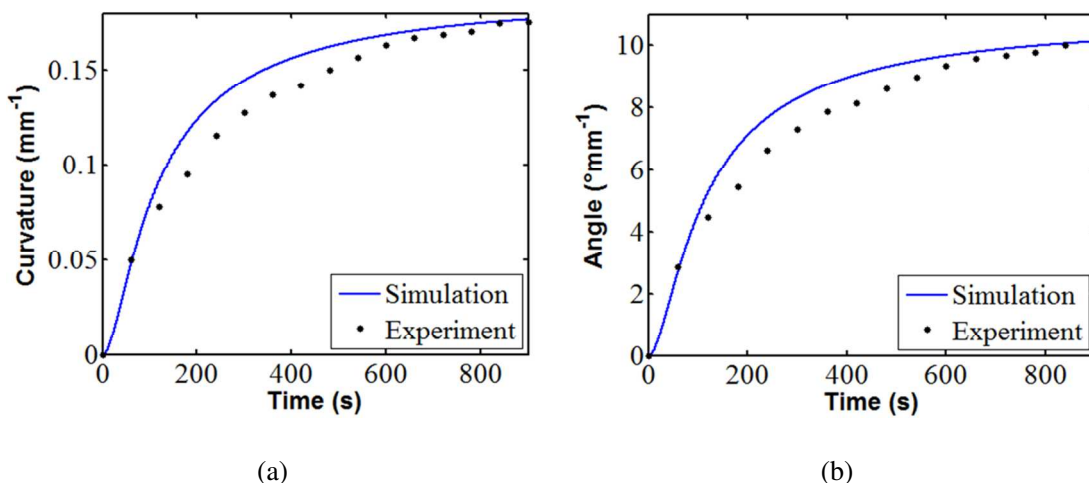
Figure 5. Simulation and experimental results: (a) bending curvature; (b) bending angle.

Based on our experimental observations, the laminated composite design can be activated successfully in a free-standing state and exhibits noticeable bending behavior. However, the bending curvature at this point is not large enough to be used for the general design of photo-origami, where creases approaching those of paper-based origami are desired. Therefore, a parametric study examining the effects of the geometric and material properties is presented in the next subsection to explore the design space that can be used in photo-origami.

4.3 Parametric study

The theoretical model for laminate design provides a tool to explore the design space, which is prescribed by the laminate geometric parameters and the material properties. Based on the parametric study and the current laminated composite properties, the bending angle can indeed be improved.

To show the interrelationship between the laminate geometry, the material property and the bending angle in detail, we set the modulus ratio and the thickness ratio between the intermediate NOA 65 layer and the LAP layer as *x*- and *y*- axes, respectively, while on the *z*- axis we plot the bending angle as shown in the 3D plots on the left of Figure 6. In

the 2D plots, on the right side of Figure 6, four curves with the specific thickness ratios

(0.5, 1.0, 1.5, and 2.0) are compared to provide a better visual picture.
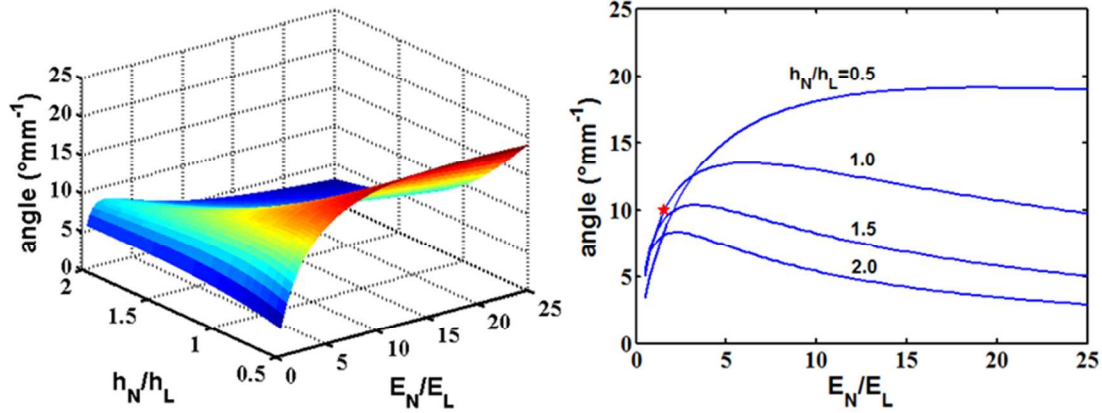
(a)
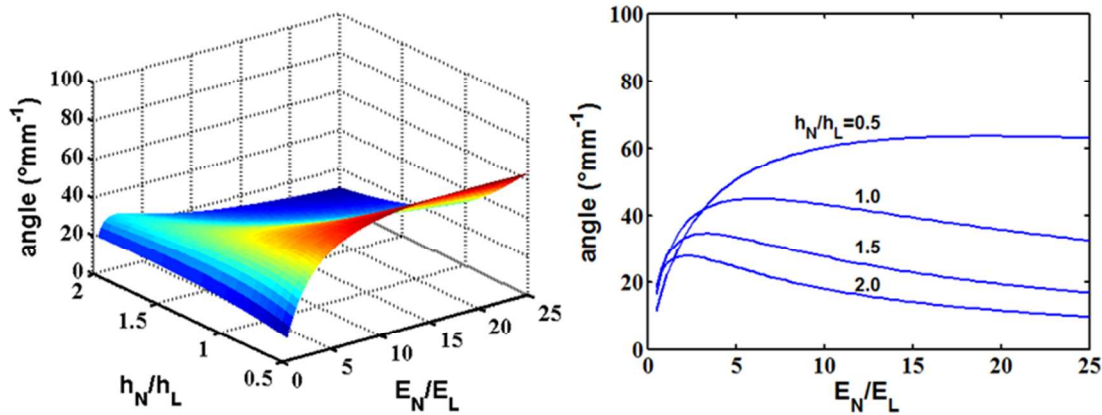
(b)
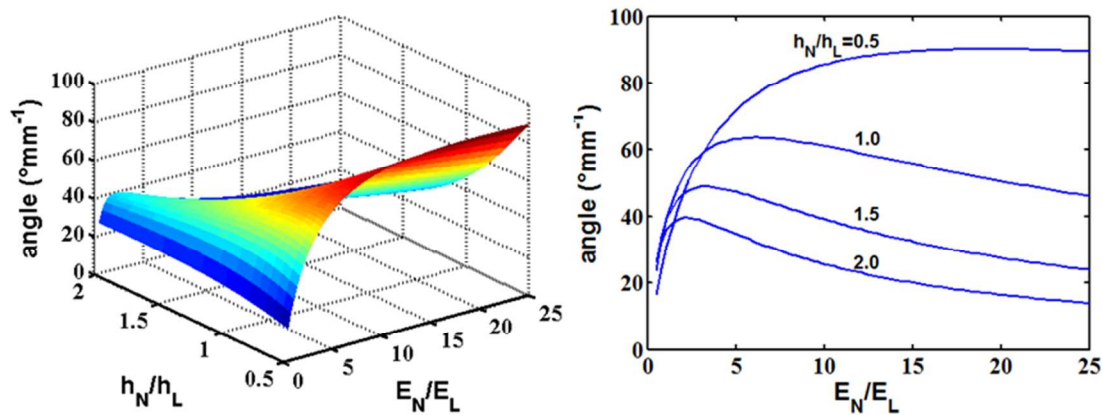
(c)

Figure 6. 3D and 2D plots showing the bending angle varying with thickness ratios and modulus ratios, using different initial strains in the intermediate NOA65 layer and different thickness of the LAP layer: (a) $\varepsilon_0 = 15\%, h_L = 0.17$ mm. The red star shows the current design; (b) $\varepsilon_0 = 50\%, h_L = 0.17$ mm; (c) $\varepsilon_0 = 50\%, h_L = 0.12$ mm.

In Figure 6a, the thickness of the LAP layer is 0.17 mm and the initial strain in the intermediate layer is 15%. The current laminate bending experiment shown in Figure 4 used the same strain and thickness with the thickness ratio $E_N/E_L = 1.0$ and is shown as a reference point (star) on the 2D plot. It is interesting to note that there is a nonlinear relationship between the modulus of the intermediate layer and the bending angle. Increasing the intermediate layer elastic modulus initially increases the bending angle because that leads to increasing compression of the LAP layer more (for a given strain), in turn leading to more bending during light activation. However, since the intermediate layer also provides resistance to bending (even though it crosses the mid-plane for bending), too high of an elastic modulus for the intermediate layer will eventually reduce the bending angle. It is also important to note that the bending angle decays dramatically with the increase of the thickness ratio in the selected range because the thicker the intermediate layer is, the larger its cross-section area will be and the more resistant to bending it will become. In this case, for the thickness ratio above 2.0, the bending angle keeps decreasing until approaches to zero since LAPs play a negligible role, mechanically, when the thickness ratio is enormously large. However, for thickness ratios below 0.5 as shown in Figure S3, the bending angle decreases after reaching a critical value as a thinner intermediate layer provides a smaller compressive strain in the LAP layer and sacrifices the bending angle during irradiation.

The reason we chose this range of thickness ratios to study is for the sake of feasibility in the experiment. The lower bound of the thickness ratio 0.5 corresponds to a thickness for the intermediate layer of only about 0.08 mm. In practice, an intermediate layer as thin as 0.1 mm is already very difficult to handle during the laminate fabrication due to the fragility. The upper bound of the thickness ratio 2.0 was chosen upon observing that it was already large enough to show an obvious decay effect of the thickness ratio. Compared with the geometric and material properties of the current laminate, we conclude that a stiff and thin intermediate layer is favorable. Noting that NOA-65's elastic modulus is 6.7 MPa, there is room for improvement.

The initial strain in the intermediate layer has a major effect on the bending angle as shown in Figure 6b. With an initial strain 50% in the intermediate layer, it is able to create a bending angle as large as $65^{o}\,\mathrm{mm}^{-1}$ in the laminated composite. This is because a larger initial strain in the intermediate layer helps compress the LAP layer, introducing a larger compressive stress by its contraction. Therefore, the stress relaxed in the irradiated LAP layer is predicted to increase, generating a larger stress mismatch thus creating a larger bending angle in the laminated composite.

Based on the theoretical model, the individual modulus of each layer does not affect the final bending angle results as long as the modulus ratio is fixed. However, unlike the modulus ratio, a fixed thickness ratio does generate different bending angles if the thicknesses of individual layers change. As shown in Figure 6c, a slightly thinner (0.12mm) LAP layer can create a bending angle as large as $90^{o}\,\mathrm{mm}^{-1}$, which can be utilized to fold a hinge in photo-origami. Therefore, a larger bending angle can also be achieved by isotropically scaling down the size of the laminated composite, establishing our principle challenge to be one of manufacturing.

A laminate design has been demonstrated to be feasible for photo-bending without external loading and our parametric studies provide the theoretical foundation for

enhancing the bending curvature. However, there are some challenges to achieve a large bending curvature in order to better meet requirements for origami applications. One is the limited adhesion between the intermediate layer and the LAP layer: delamination was found to occur for the cases with an initial strain larger than 15%. Indeed in earlier experiments, we used PDMS as the intermediate layer and achieved photo-induced bending in the laminate. However, the adhesion between PDMS and LAPs was so weak that the laminate usually delaminated after unloading; i.e., before photo-actuation could be attempted. NOA65 was selected as a better choice for the intermediate layer due to its thiol-ene reaction that provides a stronger adhesion. Moreover, attributed to its large modulus, NOA65 yielded a larger bending curvature than PDMS. Another potential challenge is the oxygen inhibition near the surface of a film [39]. This inhibitory effect of molecular oxygen inactivates radicals during photopolymerization and may also decay the rate of BERs, preventing LAPs from relaxing more stress, and diminishing the bending curvature of the laminated composite. To solve these problems, we are searching for other substitute elastomers as the intermediate layer and testing the oxygen effect on BERs in LAPs.

5   Conclusions

A light-activated polymer laminated composite was designed to overcome the drawback of prior approaches that required mechanical loading during irradiation. A theoretical model was also developed to assist the design. Experimentally, we observed that illumination of one side of the laminate gradually curled the samples toward the light to a limiting value. The theoretical model developed was successful in predicting the features of the observed bending angle and fits the experimental observations well. A parametric study explored the laminate design space in geometric and material properties. The results of this study indicated that a thin intermediate layer with a large modulus

compared to that of the LAP layer produces a large bending curvature. Other effective methods to gain a significantly enhanced bending curvature include increasing the initial strain in the intermediate layer, isotropic scaling down the size of the laminated composite.

Acknowledgement

References

1.   Broer, D.J., et al., *Photo-induced diffusion in polymerizing chiral-nematic media.* Advanced Materials, 1999. **11**(7): p. 573-+.

2.   White, T.J., et al., *A high frequency photodriven polymer oscillator.* Soft Matter, 2008. **4**(9): p. 1796.

3.   van Oosten, C.L., et al., *Bending Dynamics and Directionality Reversal in Liquid Crystal Network Photoactuators.* Macromolecules, 2008. **41**(22): p. 8592-8596.

4.   White, T.J., et al., *Polarization-controlled, photodriven bending in monodomain liquid crystal elastomer cantilevers.* Journal of Materials Chemistry, 2009. **19**(8): p. 1080.

5.   White, T.J., et al., *Widely tunable, photoinvertible cholesteric liquid crystals.* Adv Mater, 2011. **23**(11): p. 1389-92.

6.   Liu, D., et al., *Photo-switchable surface topologies in chiral nematic coatings.* Angew Chem Int Ed Engl, 2012. **51**(4): p. 892-6.

7.   Liu, D., et al., *(Photo-)thermally induced formation of dynamic surface topographies in polymer hydrogel networks.* Langmuir, 2013. **29**(18): p. 5622-9.

8.   Ikeda, T., et al., *Anisotropic bending and unbending behavior of azobenzene liquid-crystalline gels by light exposure.* Advanced Materials, 2003. **15**(3): p. 201-+.

9.   Lee, K.M., et al., *Light-activated shape memory of glassy, azobenzene liquid crystalline polymer networks.* Soft Matter, 2011. **7**(9): p. 4318-4324.

10.   Andreas Lendlein, H.J., Oliver Ju¨ nger & Robert Langer, *Light-induced shape-memory polymers.* Nature, 2005. **434**(7035): p. 876-9.

11.   Mather, P.T., X. Luo, and I.A. Rousseau, *Shape Memory Polymer Research.* Annual Review of Materials Research, 2009. **39**(1): p. 445-471.

12.   Scott, T.F., et al., *Photoinduced plasticity in cross-linked polymers.* Science, 2005. **308**(5728): p. 1615-7.

13.   Scott, T.F., R.B. Draughon, and C.N. Bowman, *Actuation in Crosslinked Polymers via Photoinduced Stress Relaxation.* Advanced Materials, 2006. **18**(16): p. 2128-2132.

14.   Long, K.N., et al., *Light-induced stress relief to improve flaw tolerance in network polymers.* Journal of Applied Physics, 2010. **107**(5): p. 053519.

15.   Long, K.N., et al., *Photo-induced deformation of active polymer films: Single spot irradiation.* International Journal of Solids and Structures, 2011. **48**(14-15): p. 2089-2101.

16.   Kloxin, C.J., et al., *Mechanophotopatterning on a photoresponsive elastomer.* Adv Mater, 2011. **23**(17): p. 1977-81.

17.   Ma, J., et al., *A photoviscoplastic model for photoactivated covalent adaptive networks.* Journal of the Mechanics and Physics of Solids, 2014. **70**: p. 84-103.

18.   Long, K.N., M.L. Dunn, and H. Jerry Qi, *Mechanics of soft active materials with phase evolution.* International Journal of Plasticity, 2010. **26**(4): p. 603-616.

19.   Long, K.N., Dunn, M.L., Scott, T.F., Qi, H. J., *Photo-induced creep of network polymers.* International Journal of Structural Changes in Solids, 2010. **2**: p. 41-52.

20. Long, R., H.J. Qi, and M.L. Dunn, *Modeling the mechanics of covalently adaptable polymer networks with temperature-dependent bond exchange reactions.* Soft Matter, 2013. **9**(15): p. 4083.

21. Ryu, J., et al., *Photo-origami—Bending and folding polymers with light.* Applied Physics Letters, 2012. **100**(16): p. 161908.

22. Smith, J.S., *Notes on the history of origami (3rd edition).* Unpublished manuscript, 2005. http://www.bitsofsmith.co.uk/history.htm. First edition published as Booklet 1 in a series by the British Origami Society, 1972.

23. Lang, R.J., *The science of origami.* Physics World, 2007. **20**(2): p. 30-31.

24. Demaine, E.D., et al., *Folding a better checkerboard.* Algorithms and Computation, Proceedings, 2009. **5878**: p. 1074-1083.

25. Dubey, V.N. and L.S. Dai, *A packaging robot for complex cartons.* Industrial Robot-an International Journal, 2006. **33**(2): p. 82-87.

26. Wu, W.N. and Z. You, *A solution for folding rigid tall shopping bags.* Proceedings of the Royal Society a-Mathematical Physical and Engineering Sciences, 2011. **467**(2133): p. 2561-2574.

27. Randall, C.L., E. Gultepe, and D.H. Gracias, *Self-folding devices and materials for biomedical applications.* Trends in Biotechnology, 2012. **30**(3): p. 138-146.

28. Jamal, M., et al., *Simuli-responsive self-folding structures.* Abstracts of Papers of the American Chemical Society, 2012. **243**.

29. Gracias, D.H., *Stimuli responsive self-folding using thin polymer films.* Current Opinion in Chemical Engineering, 2013. **2**(1): p. 112-119.

30. Parkinson, P., et al., *Three-dimensional in situ photocurrent mapping for nanowire photovoltaics.* Nano Letters, 2013. **13**(4): p. 1405-9.

31. Liu, Y., et al., *Self-folding of polymer sheets using local light absorption.* Soft Matter, 2012. **8**(6): p. 1764.

32. Felton, S.M., et al., *Self-folding with shape memory composites.* Soft Matter, 2013. **9**(32): p. 7688.

33. Ge, Q., H.J. Qi, and M.L. Dunn, *Active materials by four-dimension printing.* Applied Physics Letters, 2013. **103**(13): p. 131901.

34. Ge, Q., et al., *Active origami by 4D printing.* Smart Materials & Structures, 2014. **23**: p. 094007-15.

35. Kloxin, C.J., T.F. Scott, and C.N. Bowman, *Stress relaxation via addition-fragmentation chain transfer in a thiol-ene photopolymerization.* Macromolecules, 2009. **42**(7): p. 2551-2556.

36. Long, K.N., et al., *Photomechanics of light-activated polymers.* Journal of the Mechanics and Physics of Solids, 2009. **57**(7): p. 1103-1121.

37. Westbrook, K.K., et al., *Constitutive Modeling of Shape Memory Effects in Semicrystalline Polymers With Stretch Induced Crystallization.* Journal of Engineering Materials and Technology, 2010. **132**(4): p. 041010.

38. Long, R., H.J. Qi, and M.L. Dunn, *Thermodynamics and mechanics of photochemcially reacting polymers.* Journal of the Mechanics and Physics of Solids, 2013. **61**(11): p. 2212-2239.

39.   Goodner, M.D. and C.N. Bowman, *Development of a comprehensive free radical photopolymerization model incorporating heat and mass transfer effects in thick films.* Chemical Engineering Science, 2002. **57**(5): p. 887-900.

27